Inorg. Chem. **2008**, *47*, 1324−1331

Iron(II) Complexes of Sterically Bulky α-Ketocarboxylates. Structural Models for α-Ketoacid-Dependent Nonheme Iron Halogenases

Seth J. Friese, Benjamin E. Kucera, Victor G. Young , Jr., Lawrence Que , Jr.,* and William B. Tolman*

Department of Chemistry and Center for Metals in Biocatalysis, University of Minnesota, 207 Pleasant Street SE, Minneapolis, Minnesota 55455

Received September 14, 2007

Reaction of the sterically hindered α-ketocarboxylate 2,6-di(mesityl)benzoylformate (MesBF) with the iron(II) complexes $LFeCl_2$ [L = *N*,*N*,*N*′,*N*′-tetramethylpropylenediamine (Me_4pda) or 6,6′-dimethyl-2,2′-bipyridine (dmby)] yielded LFe(Cl)(MesBF) (**1** or **2**). X-ray crystal structures of these complexes showed that they closely model the active site structure of the nonheme iron halogenase enzyme SyrB2. A similar synthetic procedure using benzoylformate with L = dmby yielded (dmby)Fe[(O_2CC(O)Ph)]$_2$ (**3**) instead, demonstrating the need for the sterically hindered α-ketocarboxylate to assemble the halogenase model compounds. In order to make reactivity comparisons among the structurally related iron(II) complexes of benzoylformates of varying steric properties, the complexes [LFe(O_2CC(O)Ar)]$_n$ (**4**−**6**) were prepared, where L′ = tris(pyridylmethyl)amine (tpa) and Ar = 2,6-dimesitylphenyl, 2,6-di*p*-tolylphenyl, or 2,4,6-trimethylphenyl, respectively. X-ray structures for the latter two cases (**5** and **6**) revealed dinuclear topologies (n = 2), but UV–vis and ^{1}H NMR spectroscopy indicated that all three complexes dissociated in varying degrees to monomers in CH_2Cl_2 solution. Although compounds **1**−**6** were oxidized by O_2, oxidative decarboxylation of the α-ketocarboxylate ligand(s) only occurred for **3**. These results indicate that the steric hindrance useful for structural modeling of the halogenase active site prohibits functional mimicry of the enzyme.

Introduction

A large and functionally diverse set of enzymes that activate dioxygen for oxygenation of organic substrates has a common monoiron active site supported by the so-called "2-His-1-carboxylate facial triad" that leaves open three coordination sites for binding of substrate and O_2 during catalysis.[1–4] Recently, this class has been extended[5] by the discovery of nonheme iron halogenases in which the carboxylate is replaced by a halide.[6,7] These halogenase enzymes are homologous to those that use O_2 and α-ketoglutarate (α-KG) to perform substrate oxidations, and similar mechanisms for generation of the proposed Fe^{IV}═O active oxidant have been proposed (Figure 1). According to the currently favored hypotheses, a 5-coordinate Fe^{II} center with the α-KG cofactor bound in bidentate fashion (**A**) reacts with O_2 to yield an Fe—O_2 adduct (**B**). Subsequent intramolecular attack by the bound O_2 motiety at the α-carbon of α-KG induces decarboxylation to yield CO_2, succinate, and an Fe^{IV}═O unit (**C**). Here, the pathway diverges for the different types of enzymes. For those with the 2-His-1-carboxylate facial triad, the Fe^{IV}═O moiety oxidizes substrate via an oxygen rebound-type pathway, whereas for the halogenases, transfer of the halogen ligand occurs instead of oxygen rebound.[8] The apparent link between the specific iron(II) ligation and differing enzymatic function raises many questions about structure/function relationships in these systems that current research aims to address.

Synthetic model studies have provided important insights into the mechanisms of α-KG-dependent iron active sites.[1]

* To whom correspondence should be addressed. E-mail: que@chem.umn.edu (L.Q.), tolman@chem.umn.edu (W.B.T.).

(1) Costas, M.; Mehn, M. P.; Jensen, M. P.; Que, L., Jr. *Chem. Rev.* **2004**, *104*, 939–986.
(2) Abu-Omar, M. M.; Loaiza, A.; Hontzeas, N. *Chem. Rev.* **2005**, *105*, 2227–2252.
(3) Koehntop, K. D.; Emerson, J. P.; Que, L., Jr. *J. Biol. Inorg. Chem.* **2005**, *10*, 87–93.
(4) Purpero, V.; Moran, G. R. *J. Biol. Inorg. Chem.* **2007**, *12*, 587–601.
(5) Straganz, G. D.; Nidetzky, B. *ChemBioChem* **2006**, *7*, 1536–1548.
(6) Vaillancourt, F. H.; Yeh, E.; Vosburg, D. A.; Garneau-Tsodikova, S.; Walsh, C. T. *Chem. Rev.* **2006**, *106*, 3364–3378.
(7) Blasiak, L. C.; Vaillancourt, F. H.; Walsh, C. T.; Drennan, C. L. *Nature* **2006**, *440*, 368–371.
(8) Galonic, D. P.; Barr, E. W.; Walsh, C. T.; Bollinger, J. M.; Krebs, C. *Nat. Chem. Biol.* **2007**, *3*, 113–116.

10.1021/ic701823y CCC: $40.75 © 2008 American Chemical Society
Published on Web 01/25/2008

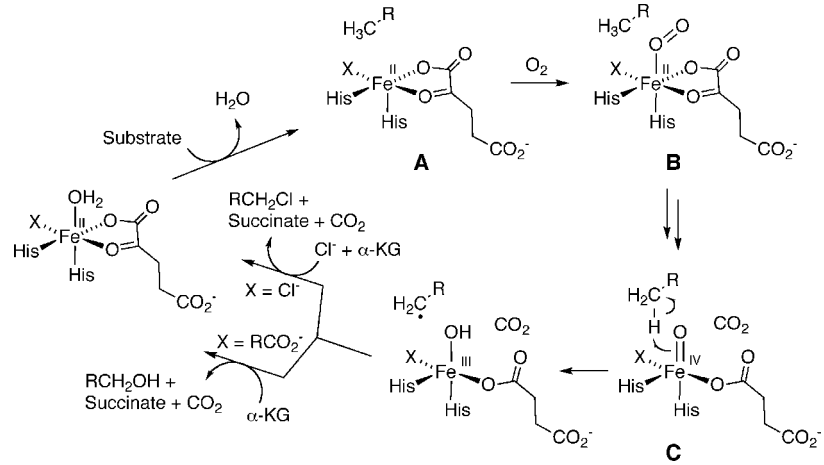

Figure 1. Proposed mechanisms for α-KG-dependent enzymes, showing similar oxygen activation steps (**A** → **C**) but divergent substrate oxidation routes depending on the nature of X (halide vs carboxylate).

Pertinent examples include the structural characterization of iron(II)-benzoylformate complexes supported by tri- and tetradentate N-donor ligands that model the proposed α-KG coordination in the enzymes[9,10] and the observation of biomimetic decarboxylation/oxidation chemistry upon oxygenation in some cases.[9,11,12] Models of the halogenase active site have yet to be prepared. Using a strategy involving application of sterically hindered terphenyl-carboxylate ligands to control complex nuclearity and facilitate isolation of reactive intermediates through hydrophobic encapsulation,[13,14] we recently reported the preparation of mononuclear zinc(II) and iron(II) complexes $LM(O_2CR)Cl$ (L = alkylated diamine, M = Zn, Fe, R = terphenyl group) that feature flexible N,N,O(carboxylate) ligation akin to that provided by the 2-His-1-carboxylate facial triad.[15] Viewing the complexes from another perspective, we envisioned that replacement of the carboxylate ligand with an α-ketocarboxylate would generate replicas of the halogenase intermediate **A**. Herein, we report the synthesis of sterically bulky terphenyl-substituted α-ketocarboxylates and their successful use for the synthesis of such accurate models of **A**. In addition, we have compared the properties and O_2 reactivity of complexes of the parent benzoylformate, including previously reported ones supported by tris(pyridylmethyl)amine (tpa),[9] with analogs prepared using sterically hindered α-ketocarboxylates. These studies have revealed important consequences of α-ketocarboxylate substituent variation on their biomimetic iron(II) chemistry.

Results and Discussion

(a) Synthesis. The sterically bulky 2,6-di(aryl)benzoic acids (aryl = mesityl or p-tolyl) were prepared from 2,6-di(aryl)iodobenzene via lithiation, reaction with ethyl chlorooxoacetate, and basic hydrolysis of the resulting esters (Scheme 1).[16,17] Addition of thallium acetate to aqueous suspensions of the α-ketoacids according to an established procedure[18] yielded the thallium salts Tl[2,6-di(mesityl)benzoylformate] (Tl-MesBF) and Tl[2,6-di(*p*-tolyl)benzoylformate] (Tl-*p*-tolylBF) as analytically pure solids in overall yields of 58% and 57%, respectively. Reasoning that its high degree of steric encumbrance would favor formation of mononuclear iron(II) complexes containing a single α-ketocarboxylate, we added 1 equiv of Tl-MesBF to $(Me_4pda)FeCl_2$ (Me_4pda = *N*,*N*,*N*′,*N*′-tetramethylpropylenediamine)[19] or $(dmby)FeCl_2$ (dmby = 6,6′-dimethyl-2,2′-bipyridine)[20] in CH_2Cl_2. Removal of precipitated TlCl and recrystallization provided purple or red complexes **1** (90%) or **2** (45%),

Scheme 1. Synthesis of Terphenyl α-Ketocarboxylates and Complexes **1** and **2**

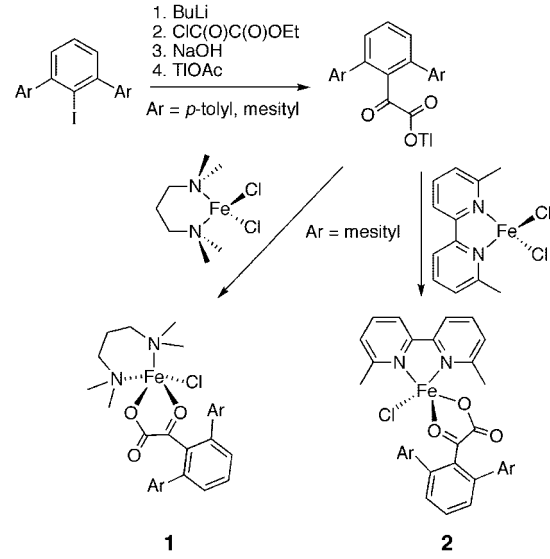

(9) Chiou, Y.-M.; Que, L., Jr. *J. Am. Chem. Soc.* **1995**, *117*, 3999–4013.
(10) Hikichi, S.; Ogihara, T.; Fujisawa, K.; Kitajima, N.; Akita, M.; Morooka, Y. *Inorg. Chem.* **1997**, *36*, 4539–4547.
(11) Mehn, M. P.; Fujisawa, K.; Hegg, E. L.; Que, L., Jr. *J. Am. Chem. Soc.* **2003**, *125*, 7828–7842.
(12) Ha, E. H.; Ho, R. Y. N.; Kisiel, J. F.; Valentine, J. S. *Inorg. Chem.* **1995**, *34*, 2265–2266.
(13) Que, L., Jr.; Tolman, W. B. *J. Chem. Soc., Dalton Trans.* **2002**, 653–660.
(14) Tshuva, E. Y.; Lippard, S. J. *Chem. Rev.* **2004**, *104*, 987–1012.
(15) Friese, S. J.; Kucera, B. E.; Que, L.; Tolman, W. B. *Inorg. Chem.* **2006**, *45*, 8003–8005.
(16) Nimitz, J. S.; Mosher, H. S. *J. Org. Chem.* **1981**, *46*, 211–213.
(17) Chen, Y. T.; Seto, C. T. *J. Med. Chem.* **2002**, *45*, 3946–3952.
(18) Müller, R.; Hübner, E.; Burzlaff, N. *Eur. J. Inorg. Chem.* **2004**, 2151–2159.
(19) Handley, D. A.; Hitchcock, P. B.; Lee, T. H.; Leigh, G. J. *Inorg. Chim. Acta* **2001**, *314*, 14–21.

Scheme 2. Synthesis of Complex **3**

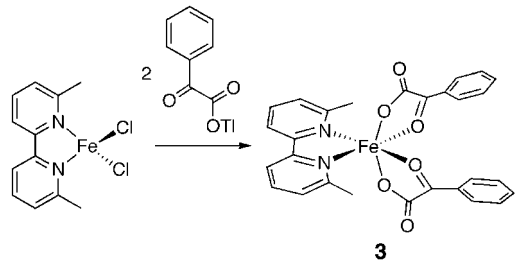

Scheme 3. Synthesis of Complexes **4**–**6**

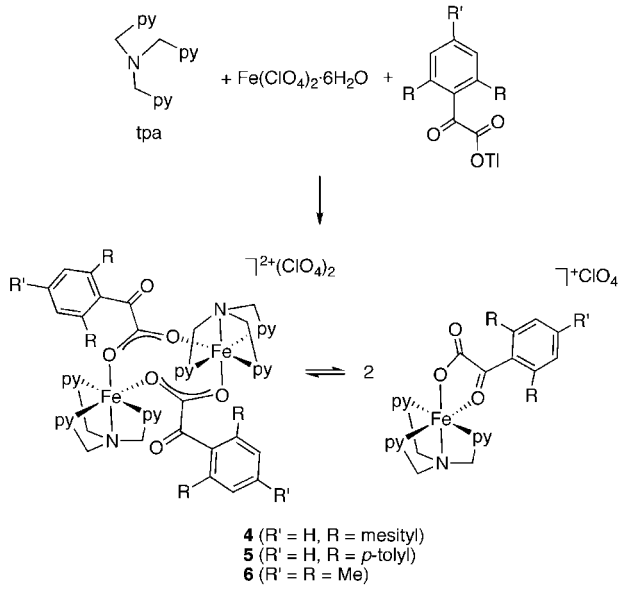

respectively. These compounds were fully characterized by X-ray crystallography, spectroscopy (UV–vis, NMR, IR) and elemental analysis (C,H,N). The steric bulk of Tl-MesBF is key to the syntheses, as indicated by the finding that reaction of thallium benzoylformate with (dmby)$FeCl_2$ yields the bis(benzoylformate) complex **3** (Scheme 2). Use of 1:1 molar ratios of the reagents in this synthesis rather than the optimized 2:1 ratio led to a mixture comprised mostly of **3** and unreacted (dmby)$FeCl_2$, with only a small amount (<10%) of another species (tentatively identified as an analog of **1** and **2**) observable by ^{1}H NMR spectroscopy.

In order to draw comparisons among the reactivity of structurally related iron(II) complexes of benzoylformates of varying steric properties, in particular to the previously published complex (tpa)Fe(BF) (BF = benzoylformate),[9] we targeted analogs by mixing tpa, $Fe(ClO_4)_2$·$6H_2O$, and Tl-MesBF, Tl-p-toylBF, or Tl[2,4,6-trimethylbenzoylformate] (Tl-Me_3BF) (Scheme 3). The products isolated (**4**–**6**, 79–89% yields) are drawn as equilibrating mixtures of mono- and dinuclear complexes on the basis of X-ray crystallographic data for **5** and **6** that show dinuclear structures and UV–vis and electrospray mass spectrometry data that suggest that monomeric species with bidentate α-ketocarboxylate coordination form to some extent in solution (see below).

(20) (a) Chan, B. C. K.; Baird, M. C. *Inorg. Chim. Acta* **2004**, *357*, 2776–2782. (b) Yang, P.; Chan, B. C. K.; Baird, M. C. *Organometallics* **2004**, *23*, 2752–2761.

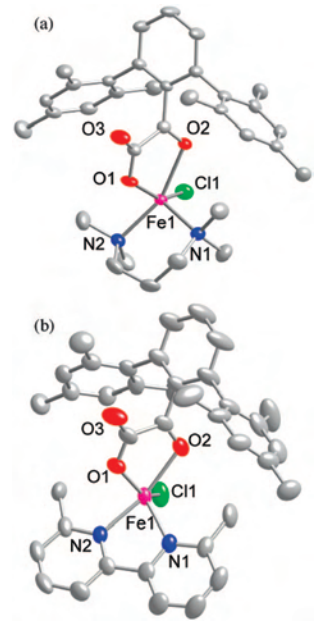

Figure 2. X-ray structural representations of (a) **1** and (b) **2**, with all atoms shown as 50% thermal ellipsoids and hydrogen atoms omitted for clarity.

(b) X-ray Structures. Representations of the X-ray crystal structures of complexes **1**−**3** and **6** are shown in Figures 2−5, while that of **5** (which is quite similar to **6**) is presented in Figure S1 in the Supporting Information. Selected bond distances and angles for all structures are listed in Table 1.

In **1** and **2**, the α-ketocarboxylate ligand binds in a bidentate fashion to a 5-coordinate Fe(II) ion, with a chloride and the bidentate N-donor ligand completing the coordination sphere (Figure 2). The geometries are distorted from square pyramidal to differing extents, as reflected by τ values of 0.13 and 0.38 for **1** and **2**, respectively (values of 0 and 1 being associated with ideal square pyramidal or trigonal bipyramidal geometries, respectively).[21] The greater proximity of **1** to square pyramidal may be traced to the larger chelate ring size for Me_4pda than for dmby. As reported previously for other complexes that feature bidentate α-ketocarboxylate coordination,[1,9,10] the Fe−O1(carboxylate) bond distances (2.014(3) for **1** and 1.995(2) Å for **2**) are shorter than the Fe−O2(keto) distances (2.292(2) for **1** and 2.282(2) Å for **2**). Because of steric interactions involving the mesityl rings, the central aryl ring of the terphenyl unit is oriented far from coplanarity with the α-ketocarboxylate plane (∼70°). As a result, the appended mesityl rings encapsulate the α-ketocarboxylate group in a manner that we postulate has important implications for O_2 reactivity (see below).

Overall, the structures of **1** and **2** replicate key features of the active site of the halogenase SyrB2,[7] with the more square pyramidal site of **1** more closely approximating that of the enzyme (Figure 3). There are significant differences between the structures with respect to Cl ligation: the Fe−Cl distances (2.44 Å in SyrB2 vs 2.2653(10) Å in **1** and 2.2646(8) Å in **2**) and the relative disposition of the chloride and α-ketocarboxylate ligands (carboxylate O cis to chloride in SyrB2

(21) Addison, A. W.; Rao, T. N.; Reedijk, J.; van Rijn, J.; Verschoor, G. C. *J. Chem. Soc., Dalton Trans.* **1984**, 1349–1356.

Table 1. Selected Bond Distances (Å) and Angles (deg) for Complexes Characterized in This Study[a]

	(Me$_4$pda)Fe(MesBF)Cl (**1**)		
Fe1−N1	2.159(3)	Fe1−N2	2.192(3)
Fe1−O1	2.014(3)	Fe1−O2	2.292(2)
Fe1−Cl1	2.2653(10)		
O1−Fe1−N1	99.16(11)	O1−Fe1−N2	87.70(10)
N1−Fe1−N2	98.20(11)	O1−Fe1−Cl1	149.49(8)
N1−Fe1−Cl1	108.31(8)	N2−Fe1−Cl1	100.94(8)
O1−Fe1−O2	74.84(9)	N1−Fe1−O2	98.78(10)
N2−Fe1−O2	157.32(10)	Cl1−Fe1−O2	87.84(7)
	(dmby)Fe(MesBF)Cl (**2**)		
Fe1−O1	1.9949(18)	Fe1−N1	2.122(2)
Fe1−N2	2.144(2)	Fe1−Cl1	2.2646(8)
Fe1−O2	2.2817(19)		
O1−Fe1−N1	113.21(8)	O1−Fe1−N2	86.35(8)
N1−Fe1−N2	77.47(8)	O1−Fe1−Cl1	137.82(6)
N1−Fe1−Cl1	108.91(6)	N2−Fe1−Cl1	105.11(6)
O1−Fe1−O2	74.41(8)	N1−Fe1−O2	107.96(8)
N2−Fe1−O2	160.65(8)	Cl1−Fe1−O2	90.88(6)
	(dmby)Fe(BF)$_2$ (**3**)		
Fe1−O4	2.0139(17)	Fe1−O1	2.0190(17)
Fe1−N2	2.166(2)	Fe1−N1	2.172(2)
Fe1−O6	2.3343(17)	Fe1−O3	2.3350(17)
O4−Fe1−O1	157.40(7)	O4−Fe1−N2	102.26(7)
O1−Fe1−N2	95.28(7)	O4−Fe1−N1	92.31(7)
O1−Fe1−N1	105.52(7)	N2−Fe1−N1	77.14(8)
O4−Fe1−O6	74.03(6)	O1−Fe1−O6	87.33(6)
N2−Fe1−O6	107.14(7)	N1−Fe1−O6	166.21(7)
O4−Fe1−O3	87.50(6)	O1−Fe1−O3	74.32(7)
N2−Fe1−O3	169.50(6)	N1−Fe1−O3	106.65(7)
O6−Fe1−O3	71.55(6)		
	[(tpa)Fe(*p*-tolylBF)]$_2$(ClO$_4$)$_2$ (**5**)		
Fe1−O2	2.0298(19)	Fe1−N4	2.132(3)
Fe1−N2	2.139(3)	Fe1−N3	2.195(2)
Fe1−O1	2.2008(19)	Fe1−N1	2.255(2)
O2−Fe1−N4	106.55(9)	O2−Fe1−N2	102.09(9)
N4−Fe1−N2	150.85(10)	O2−Fe1−N3	88.00(8)
N4−Fe1−N3	91.36(9)	N2−Fe1−N3	94.99(9)
O2−Fe1−O1	103.64(8)	N4−Fe1−O1	84.39(8)
N2−Fe1−O1	83.72(9)	N3−Fe1−O1	168.32(8)
O2−Fe1−N1	164.44(8)	N4−Fe1−N1	78.29(9)
N2−Fe1−N1	75.51(10)	N3−Fe1−N1	77.00(8)
O1−Fe1−N1	91.46(8)		
	[(tpa)Fe(Me$_3$BF)]$_2$(ClO$_4$)$_2$ (**6**)		
Fe1 O1	2.0053(14)	Fe1 O2	2.1522(14)
Fe1 N2	2.1551(17)	Fe1 N4	2.1574(17)
Fe1 N3	2.2006(16)	Fe1 N1	2.2289(16)
O1−Fe1−O2	104.09(6)	O1−Fe1−N2	99.26(6)
O2−Fe1−N2	82.32(6)	O1−Fe1−N4	108.45(6)
O2−Fe1−N4	85.81(6)	N2−Fe1−N4	151.78(6)
O1−Fe1−N3	88.07(6)	O2−Fe1−N3	165.75(6)
N2−Fe1−N3	103.33(6)	N4−Fe1−N3	83.24(6)
O1−Fe1−N1	163.53(6)	O2−Fe1−N1	91.19(6)
N2−Fe1−N1	76.40(6)	N4−Fe1−N1	78.35(6)
N3−Fe1−N1	77.70(6)		

[a] Estimated standard deviations are given in parentheses.

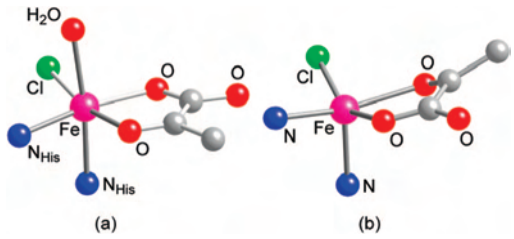

Figure 3. Comparison of the cores of (a) the active site of the halogenase SyrB2 (Protien Databank (pdb) 2FCT[7]) and (b) the model compound **1**.

vs trans in **1**). The two model complexes also lack the additional water ligand found in the enzyme structure. However, assuming that the generally accepted mechanism for α-ketoglutarate-dependent nonheme iron enzymes[1,4] applies to the halogenases, this ligand is likely to be lost upon substrate binding, so **1** and **2** may in fact be better models for the ternary enzyme–substrate−cosubstrate complex.

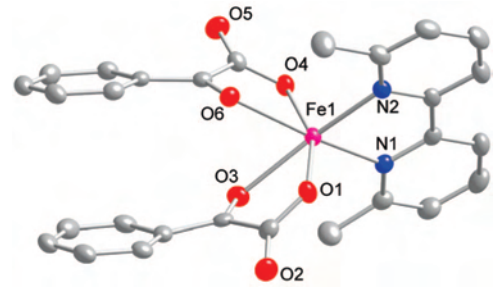

Figure 4. X-ray structure of **3**, with all atoms shown as 50% thermal ellipsoids, noncarbon atoms labeled, and hydrogen atoms omitted for clarity.

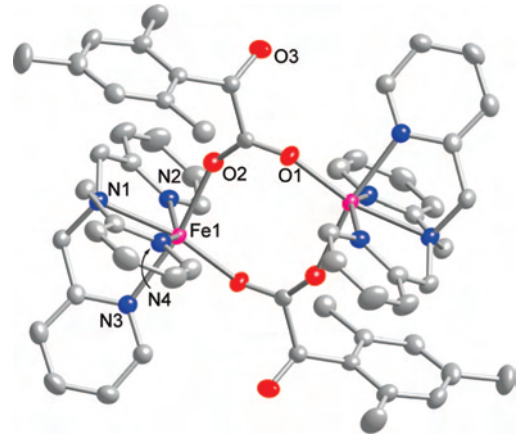

Figure 5. X-ray structural representation of the cationic portion of **6**, with all atoms shown as 50% ellipsoids, noncarbon atoms labeled, and hydrogen atoms omitted for clarity.

The X-ray structure of **3** shows bidentate coordination of two BF ligands to an Fe(II) ion, with the additional dmby ligand giving a geometry distorted relatively slightly from octahedral (Figure 4). As in **1**, **2**, and other bidentate α-ketocarboxylate complexes,[9,10] the O(carboxylate)−Fe distance is shorter than that for the O(keto)−Fe bond (Δ ∼ 0.16 Å). Interestingly, both α-ketocarboxylate chelate rings are distorted from planarity, apparently to accommodate stacking of the arene substuents, both within the same molecule and with neighbors in the crystal lattice (see packing diagrams in Figure S2 in the Supporting Information). In an important contrast with **1** and **2**, these aryl groups are essentially coplanar with their respective α-keto units, leaving the latter relatively accessible to nucleophilic attack compared to those in **1** and **2** that are almost entirely enclosed by the mesityl substituents of the MesBF ligand.

Complexes **5** (Figure S1) and **6** (Figure 5) have analogous structures that feature two octahedral Fe(II) ions bound to tetradentate tpa ligands and bridged by the carboxylates of their respective α-ketocarboxylates. We were unable to obtain crystals of **4** suitable for X-ray diffraction studies. For **5** and **6**, an inversion center relates each half of the dimeric molecule, which have similar Fe···Fe separations of ∼4.65 Å and overall topologies analogous to that reported for [(tpa)$_2$Fe(O$_2$CCH$_3$)$_2$](BPh$_4$)$_2$.[22] These dimeric structures

(22) Ménage, S.; Zang, Y.; Hendrich, M. P.; Que, L., Jr. *J. Am. Chem. Soc.* **1992**, *114*, 7786–7792.

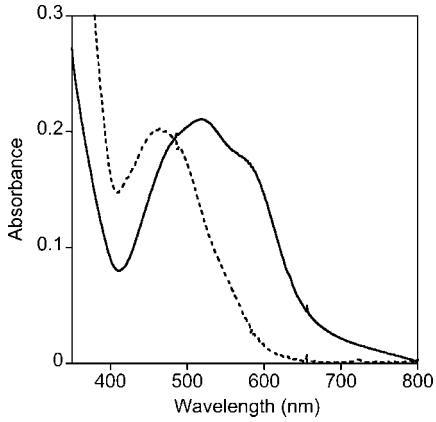

Figure 6. UV–vis spectra of 1.0 mM solutions (CH_2Cl_2) of **1** (solid line) and **2** (dashed line).

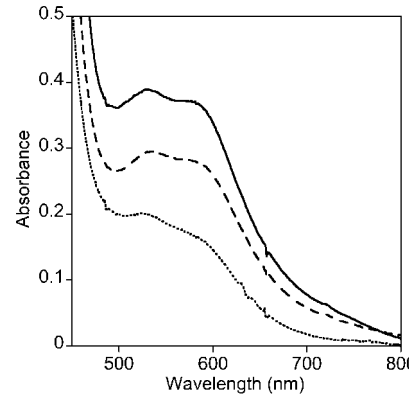

Figure 7. UV–vis spectra of 1.0 mM solutions (CH_2Cl_2) of **4** (solid line), **5** (dashed line), and **6** (dotted line).

distinctly contrast with the monomeric ones reported previously for BF complexes supported by tpa and tris(6-methylpyridylmethyl)amine (6-Me_3-TPA),[9] which presumably results from the greater steric demands of the MesBF, *p*-tolylBF, and Me_3BF ligands. An apparent consequence of the bridging carboxylate binding mode of the α-ketocarboxylates in **5** and **6** is positioning of the keto group out of coplanarity with the carboxylate; in **6**, the torsional angle O1−C1−C2−O3 is 35.8(4)°, while in **5** it is 54.1(3)°. Finally, we note that the dimeric structures for **4**–**6** appear to be disrupted in solution, as discussed below.

(c) Properties in Solution. UV–vis and ^{1}H NMR spectroscopic data for complexes **1** and **2** in CH_2Cl_2 or CD_2Cl_2 indicate that they maintain their structural integrity to a large extent in solution, albeit not entirely. They exhibit purple and red colors, respectively, that are characteristic for an α-ketocarboxylate bound in bidentate fashion to an Fe(II) center.[9,11,23,24] In the UV–vis spectrum of **1**, three peaks with approximate λ_{max} values of 488, 523, and 587 nm ($\varepsilon \sim 210$, 200, and 150 M^{-1} cm^{-1}, respectively; Figure 6) are observed, while, for **2**, closely overlapping peaks appear with λ_{max} values of about 458, 483, and 547 nm ($\varepsilon \sim 220$, 200, and 80 M^{-1} cm^{-1}, respectively). By analogy to previously reported data,[9,11,23,24] we attribute these features to Fe(II) → α-ketocarboxylate MLCT transitions. The shift to lower wavelength (higher energy) of the features for **2** is consistent with the greater Lewis acidity of the Fe(II) ion in this complex that arises from poorer electron donation from the supporting dmby donor relative to Me_4pda. The extinction coefficients for these bands in both complexes are low compared to those for complexes with simple benzoylformates (∼540 M^{-1} cm^{-1})[11] but are similar to those of an aliphatic α-ketocarboxylate complex (∼220 M^{-1} cm^{-1})[11] and the α-KG complexes of several proteins.[24,25] The higher extinctions for the parent BF case were attributed to conjugation of the α-ketocarboxylate functionality with the aryl group, which is absent in the aliphatic examples. Similarly, this conjugation is lacking for MesBF in **1** and **2** because of the large steric profile of the mesityl groups, which causes the central aryl ring to be almost orthogonal to the α-ketocarboxylate plane (Figure 2). ^{1}H NMR spectra also indicate that intact complexes **1** and **2** are the predominate species in CD_2Cl_2 solution, but a small amount (∼20%) of disproportionation to $LFeCl_2$ and $LFe(MesBF)_2$ (L = Me_4pda or dmby) is evident; this is most clearly illustrated in the spectrum for **2** (Figure S3 in the Supporting Information, where the assignment for (dmby)$Fe(MesBF)_2$ is based on the similarity of the peaks for the dmby ligand to those of **3**).

UV–vis spectra of **4**–**6** (Figure 7) also exhibit Fe(II) → α-ketocarboxylate metal-to-ligand charge transfer (MLCT) transitions indicative of bidentate α-ketocarboxylate coordination and, thus, adoption of monomeric structures in solution. The intensities differ, however, suggesting that either (a) the degree of dissociation varies (**4** > **5** > **6**) or (b) all of the complexes exist as monomers, but with differing proportions of mono- and bidentate α-ketocarboxylate coordination. With the data currently available, we cannot distinguish between these possibilities. However, the fact that the apparent extinction coefficients for the visible bands fall within the range found for mononuclear iron(II) complexes with bidentate α-ketocarboxylate coordination reported thus far[11] suggests that species with bidentate α-ketocarboxylate coordination represent at least one-third of the molecules present in solution, so there is significant dissociation of the dinuclear structures found in the crystals. Further support for the presence of monomers is apparent in the ESI-MS data, exemplified for **4** in Figure S4 in the Supporting Information, which shows the appropriate *m*/*z* and isotope pattern for $[Fe^{II}(tpa)(MesBF)]^+$. The ^{1}H NMR spectrum for each complex (Figure S5) contains a single set of peaks for the TPA protons (paramagnetically shifted as in other TPA−Fe^{II} compounds[9]) and for those associated with the α-ketocarboxylate. Together, the UV–vis and NMR data are best interpreted to indicate that the compounds are highly fluxional in solution, with interconversions between mono- and dinuclear structures and/or mono- and bidentate α-ketocarboxylate coordination modes being rapid on the NMR time scale. Importantly for O_2 reactivity studies, the UV–vis

(23) Ho, R. Y. N.; Mehn, M. P.; Hegg, E. L.; Liu, A.; Ryle, M. J.; Hausinger, R. P.; Que, L., Jr. *J. Am. Chem. Soc.* **2001**, *123*, 5022–5029.
(24) Pavel, E. G.; Zhou, J.; Busby, R. W.; Gunsior, M.; Townsend, C. A.; Solomon, E. I. *J. Am. Chem. Soc.* **1998**, *120*, 743–753.
(25) Ryle, M. J.; Padmakumar, R.; Hausinger, R. P. *Biochemistry* **1999**, *38*, 15278–15286.

data confirm that each complex is able to access (to a significant extent) a structure with the bidentate α-ketocarboxylate coordination thought to be required for oxidative decarboxylation.

(d) Reactivity with O_2. All complexes studied react with dioxygen. In the case of **1**, the reactions in CH_2Cl_2, MeCN, THF, toluene, and benzene all resulted in a fading of the iron(II) chromophore followed by the formation of an insoluble red-brown precipitate (presumably iron-oxides). In contrast, when complex **2** (0.5 mmol solution in CH_2Cl_2) was exposed to dioxygen, no precipitate formed and the initially red solution became dark orange. We have been unable to isolate or characterize the final oxidized iron-containing products, but the organic ligands were recovered for analysis by adding 1 M aq. H_2SO_4 to the orange oxidized solution. The ligands were then extracted with Et_2O, washed with water, and dried with $MgSO_4$. Removal of the solvent under vacuum enabled analysis by ESI-MS and ^{1}H NMR spectroscopy. Only MesBF was observed, and there was no evidence for its oxidative decarboxylation to form 2,6-(dimesityl)benzoic acid. Similar to **2**, when complex **3** (0.5 mmol in CH_2Cl_2 or MeCN) was exposed to dioxygen, the solution turned from purple to orange without formation of a precipitate. While the final oxidized iron products could not be isolated or characterized, the ligands were recovered via the same method as that for complex **2**. Analysis by ESI-MS and ^{1}H NMR spectroscopy indicated formation of the decarboxylation product benzoic acid in 34% yield (for reaction of one BF ligand), a different outcome from that seen for complexes **1** and **2**. Unfortunately, attempts at trapping any intermediates with the exogenous substrates PPh_3, dihydroanthracene, and cumene were not successful.

Complexes **4**−**6** are bulky analogues of the complexes [(tpa)Fe(BF)(MeOH)]ClO_4 and [(6-Me$_3$-TPA)Fe(BF)]ClO_4 reported previously to undergo decarboxylation upon exposure to dioxygen in MeCN solvent at room temperature over a period of days.[9] The observed product of the reaction of [(tpa)Fe(BF)]ClO_4 with O_2 was {[Fe^{III}_2O-(tpa)$_2$-(O_2CPh)$_2$-(ClO_4)}$^+$ as monitored by FAB-MS. It was proposed that the reaction with O_2 resulted in the decarboxylation of the α-ketocarboxylate to form [(tpa)-Fe(O_2CPh)]-ClO_4 initially, which subsequently underwent further oxidation to give rise to the observed product. In contrast, the reaction of **4**, **5**, or **6** with O_2 in MeCN solvent for 2 days only resulted in the oxidation of Fe^{II} to Fe^{III} and did not give the expected oxidative decarboxylation product. Notably, ESI-MS data indicated formation of the [Fe^{III}_2-O(tpa)$_2$-(MesBF)$_2$]$^{2+}$, [Fe^{III}_2-O(tpa)$_2$-(p-tolylBF)$_2$]$^{2+}$, and [Fe^{III}_2O-(tpa)$_2$-(2,4,6-Me$_3$BF)$_2$]$^{2+}$ ions, but there was no evidence for the formation of the carboxylate analogs that would result from oxidative decarboxylation (see Figure S6 in the Supporting Information for the experimental and simulated parent ion envelope for the production of the oxygenation of **4**).

The fact that oxidative decarboxylation is not observed for any of the complexes with sterically bulky α-ketocarboxylates, despite evidence for the formation of bidentate α-ketocarboxylates, suggests that the substituents introduced into the 2 and 6 positions are preventing attack of the bound O_2 on the α-keto group, resulting only in the autoxidation of the iron(II) center. The crystal structures of **1** and **2** show that substitution at the 2 and 6 positions of the benzoate phenyl ring causes the aromatic ring to rotate out of the plane of the iron-coordinated α-ketocarboxylate. This rotation places the 2- and 6-substituents in the space above and below this plane, thereby hindering O_2 binding to the iron center and attack of the α-ketocarboxylate. Thus, while the use of bulky ortho-substituents on the α-ketocarboxylate has facilitated isolation and crystallization of suitable structural models for the active site of the iron halogenases, this very strategy ironically prevents them from acting as functional models.

Conclusion

In summary, by extending the strategy for constructing novel metal complexes using sterically hindered terphenyl carboxylate ligands[13–15] to one using similarly hindered α-ketocarboxylates, mononuclear complexes (**1** and **2**) that closely model the nonheme iron halogenase active site structure[7] have been prepared. The steric bulk of the α-ketocarboxylate substituents is key to the successful isolation of these structural model compounds, as shown by the isolation of the bis(α-ketocarboxylate) complex **3** when the unsubstituted BF was used instead. However, the steric bulk inhibits biomimetic decarboxylation by O_2, as revealed in studies of **1**, **2**, and tpa-supported diiron(II) complexes **4**–**6**. From these results it is evident that further tuning of α-ketocarboxylate structure will be required in order to access complexes that both structurally and functionally model nonheme α-ketoacid-dependent enzyme active sites.

Experimental Section

General Considerations. Manipulations were performed under an atmosphere of nitrogen using a Vacuum Atmospheres nitrogen box or employing standard Schlenk techniques, unless otherwise stated. Pentane, diethyl ether, CH_2Cl_2, and toluene were passed through a solvent purification column (Glass Contour, Laguna, CA). THF was vacuum distilled from sodium/benzophenone. Acetonitrile was vacuum distilled from calcium hydride. *N*,*N*,*N*′,*N*′-Tetramethylpropylenediamine (Me_4pda) was distilled from sodium metal. Commercial $FeCl_2$ was dried by treatment with neat Me_3SiCl. (dmby)-$FeCl_2$,[20] 2,6-dimesityliodobenzene,[26] 2,6-di(*p*-tolyl)iodobenzene,[26a] tris-(pyridylmethyl)-amine (tpa),[27] and thallium benzoylformate[18] were prepared as described in the literature. The preparation of (Me_4pda)$FeCl_2$ was carried out at room temperature instead of reflux as stated in the literature.[19] ^{1}H NMR spectra were recorded on a Varian 300 MHz or Varian 500 MHz instrument. Spectra were referenced to the residual solvent peak. Infrared spectra were obtained on a Nicolet Avatar 370 FT-IR. Elemental analyses were performed by Robertson Microlit. Inc. Data collection and structure solution for crystal structures were conducted at the X-Ray Crystallographic Laboratory, S146 Kolthoff Hall, Department of Chemistry, University of Minnesota; details are available in the CIFs.

(26) (a) Du, C. J. F.; Hart, H.; Ng, K. K. D. *J. Org. Chem.* **1986**, *51*, 3162–3165. (b) Smith, R. C.; Protasiewicz, J. D. *Eur. J. Inorg. Chem.* **2004**, 998–1006.

(27) Britovsek, G. J. P.; England, J.; White, A. J. P. *Inorg. Chem.* **2005**, *44*, 8125–8134.

Ethyl 2,6-Dimesitylbenzoylformate. To a diethyl ether solution (150 mL) containing 2,6-dimesityliodobenzene (2.11 g, 4.80 mmol), *n*-BuLi (2.5 M in hexanes, 1.95 mL) was added dropwise at room temperature and stirred for 30 min. The pale yellow solution was then cooled to −78 °C, upon which ethyl chlorooxoacetate (0.59 mL, 5.3 mmol) was added. Once the addition was complete, the yellow solution was warmed to room temperature and stirred for 18 h. A white precipitate was formed, which was removed by filtration with a glass frit. The yellow filtrate was then concentrated (ca. 10 mL) and EtOH (ca. 20 mL) was added. This procedure was repeated two more times before cooling in an ice bath, subsequently collecting the white precipitate on a glass frit, and washing twice with cold methanol (0 °C). The product (1.60 g, 81% yield) was obtained as a white solid after drying under vacuum. ^{1}H NMR (CD_2Cl_2, 300 MHz) δ 7.61 (t, 1H, J_{HH} = 7.5 Hz), 7.17 (d, 2H, J_{HH} = 7.5 Hz), 6.89 (s, 4H), 3.65 (q, 2H, J_{HH} = 7.2 Hz), 2.30 (s, 6H), 2.00 (s, 12) 0.97 (t, 3H, J_{HH} = 7.2 Hz) ppm. ^{13}C NMR (CD_2Cl_2, 75 MHz) δ 13.1, 20.0, 20.5, 61.7, 127.7, 128.9, 131.0, 135.2, 136.0, 136.5, 137.3, 140.5, 161.8, 189.0 ppm. IR (Neat): 850, 1024, 1194, 1303, 1456, 1705 (CO), 1726 (CO), 2858, 2920, 2977 cm^{-1}. Anal. calcd for $C_{28}H_{30}O_3$: C, 81.13; H, 7.29. Found: C, 80.91; H, 7.06.

Ethyl 2,6-Di*p*-tolylbenzoylformate. This compound was prepared analogously to ethyl 2,6-dimesitylbenzoylformate. The product (6.75 g, 72% yield) was obtained as a white solid after drying under vacuum. ^{1}H NMR (CD_2Cl_2, 500 MHz) δ 7.59 (t, 1H, J_{HH} = 7.5 Hz), 7.40 (d, 2H, J_{HH} = 7.5 Hz), 7.20 (dd, 8H, J_{HH} = 8.0 Hz), 3.82 (q, 2H, J_{HH} = 7.0 Hz), 2.39 (s, 6H), 0.98(t, 3H, J_{HH} = 7.0 Hz) ppm. ^{13}C NMR (CD_2Cl_2, 125 MHz) δ 13.9, 21.4, 62.8, 129.6, 129.7, 129.8, 131.0, 136.2, 137.1, 138.4, 142.4, 162.3, 191.1 ppm. IR (Neat): 713, 802, 825, 954, 1013, 1195, 1450, 1515, 1709 (CO), 1726 (CO), 2921, 2972, 3027 cm^{-1}. Anal. calcd for $C_{24}H_{22}O_3$: C, 80.32; H, 6.19. Found: C, 80.32; H, 6.09.

2,6-Dimesitylbenzoylformic Acid. To a MeOH suspension containing ethyl 2,6-dimesitylbenzoylformate (1.57 g, 4.0 mmol), 2.5 M NaOH (6 mL) was added and stirred at 50 °C for 2 h. The suspension was then cooled and conc HCl was added until the pH was about 2. The white suspension was then filtered and washed with H_2O (5 × 5 mL) and cold (0 °C) MeOH (2 × 2 mL). The product (2.60 g, 96%) was obtained as a white solid after drying under vacuum. ^{1}H NMR (CD_2Cl_2, 300 MHz) δ 7.61 (t, 1H, J_{HH} = 7.5 Hz), 7.17 (d, 2H, J_{HH} = 7.5 Hz), 6.89 (s, 4H), 5.9 (br s, 1H), 2.30 (s, 6H), 2.00 (s, 12) ppm. ^{13}C NMR (CD_2Cl_2, 75 MHz) δ 19.9, 20.5, 127.7, 128.8, 131.0, 134.8, 135.2, 136.5, 137.6, 140.2, 160.8, 190.1 ppm. IR (Neat): 656, 847, 1208, 1376, 1453, 1698, 1709, 2400–3100 (br), 2853, 2916, 2969 cm^{-1}. Anal. calcd for $C_{26}H_{26}O_3$: C, 80.80; H, 6.78. Found: C, 80.64; H, 6.78.

2,6-Di*p*-tolylbenzoylformic Acid. This compound was prepared analogously to 2,6-dimesitylbenzoylformic acid. The product (3.82 g, 86%) was obtained as a white solid after drying under vacuum. ^{1}H NMR (CD_2Cl_2, 300 MHz) δ 7.64 (t, 1H, J_{HH} = 7.5 Hz), 7.43 (d, 2H, J_{HH} = 7.5 Hz), 7.21 (d, 4H, J_{HH} = 4.5 Hz), 7.13 (d, 4H, J_{HH} = 4.5 Hz), 6.60 (br s, 1H) 2.38 (s, 6H) ppm. ^{13}C NMR (CD_2Cl_2, 75 MHz) δ 21.4, 129.6, 129.7, 129.9, 131.4, 134.2, 137.0, 138.6, 142.5, 160.6, 192.5 ppm. IR (neat): 711, 795, 820, 954, 963, 1202, 1344, 1456, 1515, 1705 (br), 2922, 3025, 2500–3300 (br) cm^{-1}. Anal. calcd for $C_{22}H_{17}O_3$: C, 79.98; H, 5.49. Found: C, 79.83; H, 5.68.

Thallium 2,6-Dimesitylbenzoylformate (Tl-MesBF). Using a precedented procedure,[18] a MeOH/water (ca. 30 mL in 1:2 ratio) suspension containing 2,6-dimesitylbenzoylformic acid (358 mg, 0.93 mmol) and thallium acetate (285 mg, 0.93 mmol) was added and stirred for 2 h. After the volatiles were removed in vacuo, ca. 30 mL of the acetone/water mixture was added again and stirred for an additional 2 h. This process was performed one more time before washing the remaining solids with ether and drying under vacuum to yield a white solid (411 mg, 0.70 mmol; 75% yield). ^{1}H NMR (DMSO-d_6, 500 MHz) δ 7.42 (t, 1H, J_{HH} = 7.5 Hz), 6.93 (d, 2H, J_{HH} = 7.5 Hz), 6.76 (s, 4H), 2.20 (s, 6H), 1.98 (s, 12) ppm. ^{13}C NMR (DMSO-d_6, 75 MHz) δ 21.6, 21.7, 128.5, 129.0, 129.9, 136.8, 137.1, 137.8, 139.5, 141.6, 166.6, 201.3 ppm. IR (neat): 850, 1213, 1362, 1453, 1592, 1676, 2849, 2916, 2946, 3048 cm^{-1}. Anal. calcd for $C_{26}H_{25}O_3Tl$: C, 52.94; H, 4.27. Found: C, 52.68; H, 4.15.

Thallium 2,6-Di*p*-tolylbenzoylformate (Tl-p-tolylBF). This compound was prepared analogously to thallium 2,6-dimesitylbenzoylformate. The product was obtained as a white solid (2.12 g, 92% yield) after drying under vacuum. ^{1}H NMR (DMSO-d_6, 300 MHz) δ 7.45 (t, 1H, J_{HH} = 7.5 Hz), 7.24 (d, 2H, J_{HH} = 7.5 Hz), 7.23 (d, 4H, J_{HH} = 7.5 Hz), 7.13 (d, 4H, J_{HH} = 7.5 Hz), 2.30 (s, 6H) ppm. ^{13}C NMR (DMSO-d_6, 75 MHz) δ 21.7, 129.1, 129.4, 129.7, 130.0, 137.1, 138.5, 140.4, 142.1, 166.5, 204.3 ppm. IR (neat): 794, 976, 1213, 1372, 1453, 1514, 1633, 1682, 2861, 2915, 3031, 3058, 3085 cm^{-1}. Anal. calcd for $C_{22}H_{17}O_3Tl$: C, 49.51; H, 3.21. Found: C, 49.28; H, 2.95.

Thallium 2,4,6-Trimethylbenzoylformate (Tl-Me$_3$BF). This compound was prepared analogously to thallium 2,6-dimesitylbenzoylformate. The product was obtained as a white solid (1.51 g, 89% yield) after drying under vacuum yielding a white solid (1.51 g, 89% yield). ^{1}H NMR (DMSO-d_6, 300 MHz) δ 6.81 (s, 2H), 2.22 (s, 3H), 2.20 (s, 6H) ppm. ^{13}C NMR (DMSO-d_6, 75 MHz) δ 20.3, 21.7, 128.9, 135.1, 138.5, 139.3, 170.0, 205.2 ppm. IR (neat): 786, 980, 1223, 1365, 1585, 1686, 2856, 2919, 2950 cm^{-1}. Anal. calcd for $C_{11}H_{11}O_3Tl$: C, 33.40; H, 2.80. Found: C, 33.29; H, 2.38.

(Me$_4$pda)Fe(MesBF)Cl (1). Thallium dimesitylbenzoylformate (100 mg, 0.17 mmol) was added to a CH_2Cl_2 solution (ca. 10 mL) containing (tmpda)$FeCl_2$ (43.6 mg, 0.17 mmol). The resulting purple solution was stirred for 10 min at room temperature. The solution was filtered and condensed to ca. 2 mL. Pentane (ca. 5 mL) was added and the solution was cooled to –20 °C overnight, which gave purple crystals (2 crops; 92 mg, 90% yield). ^{1}H NMR (CD_2Cl_2, 500 MHz) δ 166 (2H), 113 (6H), 98 (2H), 92 (6H), 8.7 (2H), 7.2 (1H), 3.2 (4H) 1.7 (12H), −0.8 (6H), −10 (1H), −16 (1H) ppm. UV–vis [δ_{max}, nm (δ, M^{-1} cm^{-1}) in CH_2Cl_2 at 20 °C]: 488 (210), 523 (200), 587 (160). IR (neat): 705, 738, 815, 854, 1222, 1327, 1610, 1683, 2840, 2916, 2962, 3009, 3052 cm^{-1}. Anal. calcd for $C_{33}H_{43}ClFeN_2O_3$: C, 65.30; H, 7.14; N, 4.62. Found: C, 65.06; H, 6.88; N, 4.46.

(dmby)Fe(MesBF)Cl (2). This compound was prepared analogously to (Me$_4$pda)Fe(MesBF)Cl. The product (45 mg, 45%) was obtained as red crystals, which became a powder after drying under vacuum. ^{1}H NMR (CD_2Cl_2, 500 MHz) δ 66 (2H), 51.0 (2H), 10.3 (2H), 7.68 (1H), 5.0 (12H), 2.50 (4H), −2.7 (6H), −12.6 (2H), −36 (6H) ppm. UV–vis [δ_{max}, nm (δ, M^{-1} cm^{-1}) in CH_2Cl_2 at 20 °C]: 458 (220), 483 (200), 547 (80). IR (neat): 705, 738, 815, 854, 1222, 1327, 1610, 1683, 2840, 2916, 2962, 3009, 3052 cm^{-1}. Anal. calcd for $C_{38}H_{37}ClFeN_2O_3$ [0.2 CH_2Cl_2(NMR)]: C, 67.67; H, 5.56; N, 4.13. Found: C, 67.62; H, 5.59; N, 4.06.

(dmby)Fe(BF)$_2$ (3). Addition of thallium benzoylformate (227 mg, 0.64 mmol) to a pale yellow CH_2Cl_2 (ca. 5 mL) solution containing (dmby)$FeCl_2$ (100 mg, 0.32 mmol) led to a dark red solution, which was stirred for 30 min. This solution was filtered and condensed (ca. 2 mL) before diethyl ether (ca. 10 mL) was added, which resulted in the immediate formation of red microcrystalline solids. These solids were collected and dried under vaccum (1.77 mg, 98% yield). Single crystals suitable for X-ray

crystallography were grown by slow evaporation of solvent from a toluene−CH_2Cl_2 mixture. ^{1}H NMR (CD_2Cl_2, 500 MHz) δ 61.0 (2H), 49.3 (2H), 15.4 (4H), 12.0 (2H), 8.42 (4H), −8.91 (2H). −23.9 (6H) ppm. IR (neat): 679, 785, 818, 1178, 1233, 1450, 1463, 1597, 1632, 1667, 2923, 3066, 3103 cm^{-1}. UV–vis [λ_{max}, nm (ε, M^{-1} cm^{-1}) in CH_2Cl_2 at 20 °C]: 485 (600), 535 (650), 585 (580). Anal. calcd for $C_{28}H_{22}FeN_2O_6$: C, 62.47; H, 4.12; N, 5.20. Found: C, 62.19; H, 4.29; N, 5.47.

[(tpa)Fe(*p*-tolylBF)]$_2$(ClO$_4$)$_2$ (5). ***Caution!*** *Perchlorate salts are prone to rapid exothermic decomposition, and appropriate care should be taken to handle carefully in small amounts.* The ligand tpa (163 mg, 0.562 mmol) was added to a MeCN solution (ca. 15 mL) containing $Fe(ClO_4)_2$•$6H_2O$ (204.3 mg, 0.563 mmol) and stirred at room temperature for 10 min. Thallium 2,6-di-*p*-tolylbenzoylformate (300 mg, 0.562 mmol) was then added, and the mixture was stirred for an additional 18 h. The solvent was removed in vacuo. The remaining residue was extracted with CH_2Cl_2 and filtered. The volatiles were removed again in vacuo before recrstalization by vapor diffusion of ether into an MeCN solution. The product (346 mg, 79% yield) was obtained as an orange solid after drying under vacuum. ^{1}H NMR (CD_2Cl_2, 500 MHz) δ 129, 71. 53, 47, 14.1, 12.1, 11.3, 10.0, 4.93, 4.39, 1.99, −0.6 ppm. UV–vis [λ_{max}, nm (ε, M^{-1} cm^{-1}) in CH_2Cl_2 at 20 °C]: 530 (320), 586 (310). IR (neat): 763, 799, 1090, 1442, 1604, 1651, 1698, 2860, 2919, 3021, 3060 cm^{-1}. Anal. calcd for $C_{80}H_{70}Cl_2Fe_2N_8O_{14}$: C, 61.99; H, 4.46; N, 7.23. Found: C, 61.73; H, 4.46; N, 7.36. HRMS(ESI) *m*/*z* calcd for [(TPA)Fe(p-tolylBF)] (M^+): 675.2054; found 675.2054.

[(tpa)Fe(MesBF)]$_2$(ClO$_4$)$_2$ (4). ***Caution!*** *Perchlorate salts are prone to rapid exothermic decomposition, and appropriate care should be taken to handle carefully in small amounts.* This compound was prepared analogously to [(tpa)-Fe-(p-tolylBF)]$_2$-$(ClO_4)_2$. The product, however, was precipitated by addition of ether into a methanol solution, which yielded the product (126 mg, 89% yield) as a green solid after drying under vacuum. ^{1}H NMR (CD_2Cl_2, 500 MHz) δ 131, 64, 54, 47, 22, 10.2, 9.5, 5.0, 4.6, 0.1 ppm. UV–vis [λ_{max}, nm (ε, M^{-1} cm^{-1}) in CH_2Cl_2 at 20 °C]: 528 (400), 572 (380). IR (neat): 622, 735, 766, 1096, 1223, 1445, 1606, 1644, 1675, 2855, 2920, 2949, 3060 cm^{-1}. HRMS-(ESI) *m*/*z* calcd for [(TPA)-Fe-(MesBF)]$^+$: 731.2680; found 731.2712.

[(tpa)Fe(Me$_3$BF)]$_2$(ClO$_4$)$_2$ (6). ***Caution!*** *Perchlorate salts are prone to rapid exothermic decomposition, and appropriate care should be taken to handle carefully in small amounts.* This compound was prepared analogously to [(tpa)Fe(*p*-tolylBF)]$_2$-$(ClO_4)_2$. The product (435 mg, 87% yield) was obtained as a orange solid after drying under vacuum. ^{1}H NMR (CD_2Cl_2, 500 MHz) δ 139, 65, 51, 49, 16.7, 8.8, 5.1, 4.9, 4.1, 2.6 ppm. UV–vis [λ_{max}, nm (ε, M^{-1} cm^{-1}) in CH_2Cl_2 at 20 °C]: 521 (160), 581 (130). IR (neat): 621, 768, 1089, 1442, 1604, 1643, 1699, 2844, 2915, 2950, 3020, 3052 cm^{-1}. Anal. calcd for $C_{58}H_{58}Cl_2Fe_2N_8O_{14}$: C, 54.69; H, 4.59; N, 8.80. Found: C, 54.79; H, 4.44; N, 8.76. HRMS(ESI) *m*/*z* calcd for [(TPA)Fe(2,4,6-trimethylBF)]$^+$: 537.1584; found 537.1609.

Reactivity with O$_2$. In a typical reaction for compounds **1** and **2**, dioxygen was bubbled through 2.5 mL solutions (0.5 mmol in CH_2Cl_2) containing compounds **1** and **2** for 10 min and allowed to react for 2 h. The organic ligands were then recovered for analysis by adding 1 M aq. H_2SO_4 (1 mL) to the orange oxidized solution. The ligands were then extracted with Et_2O (2 mL × 2), washed with water (2 mL), dried with $MgSO_4$, and filtered. The solvent was removed from the filtrate under vacuum, and the residue was analyzed by ESI-MS and ^{1}H NMR spectroscopy. Only the MesBF ligand was observed, and there was no evidence for decarboxylation of it to form 2,6-(dimesityl)benzoic acid.

Reaction of dioxygen with complex **3** was carried out under conditions similar to those used for complexes **1** and **2**, except that trimethoxybenzene was added as an internal standard. The formation of benzoate was observed in 34% yield (relative to the decarboxylation of one benzoylformate per complex) as indicated by ^{1}H NMR spectroscopic analysis (75% material recovery). The presence of benzoate was also confirmed by ESI-MS analysis.

In a typical reaction for **4**−**6**, a 1.0 mmol solution (2.5 mL) of compounds **4**, **5**, or **6** in MeCN was reacted with dioxygen by slowly bubbling O_2 into the solution for 10 min with monitoring by UV–vis spectroscopy. After the reactions were complete (within 2 days), the crude solutions were injected into the ESI mass spectrometer (positive ion mode) for analysis. Signals corresponding to$[Fe^{III}_2O(tpa)_2(MesBF)_2]^{2+}$,$[Fe^{III}_2O(tpa)_2(p\text{-}tolylBF)_2]^{2+}$,and$[Fe^{III}_2O(tpa)_2(2,4,6\text{-}Me_3BF)_2]^{2+}$ with *m*/*z* values of 545, 683, or 739, respectively, were observed, but peaks for species containing the respective products arising from oxidative decarboxylation were not apparent. Simulations of the isotope pattern for all of these ions closely matched the experimental spectra, as illustrated for the case of $[Fe^{III}_2O(tpa)_2(MesBF)_2]^{2+}$ in Figure S5 in the Supporting Information.

Supporting Information Available: Figures S1−S6 and CIF files. This material is available free of charge via the internet at http://pubs.acs.org.

IC701823Y